JOURNAL OF MATERIALS SCIENCE 29 (1994) 5158–5164

Evaluation of strength, toughness and subcritical crack extension of a commercial HP–Si_3N_4 exposed to a sulphidizing environment

C. SARAIVA MARTINS, M. STEEN
Institute for Advanced Materials, Joint Research Centre, C.E.C., P.O. Box 2, Petten, The Netherlands

L. GUERRA ROSA
CEMUL, Instituto Superior Técnico, 1096 Lisboa Codex, Portugal

Structural ceramic materials, in particular silicon nitride, have attracted interest for coal gasification technology at temperatures in excess of 1200 °C. In this study, a commercially available hot pressed silicon nitride is exposed for 200 h in a 0.4% H_2S + 0.75% H_2O + H_2 (balance) atmosphere, at 1200 and 1300 °C, simulating coal gasification environments. The crack growth behaviour of the as-received material is compared to that of the exposed condition. Measurements are carried out on specimens with small natural flaws (dynamic strength tests) and on specimens containing long cracks (chevron notch), both tested in four point bending. Results of strength tests (Modulus of rupture (MOR) and Weibull modulus) as well as toughness in both conditions are also presented. In view of the significant changes in the high temperature mechanical properties caused by crystallization of the intergranular glassy phase at triple points, further investigations of the effect of controlled devitrification seem surely worthwhile.

1. Introduction

The increase of the ISO turbine inlet temperature to 1200 or 1300 °C is of capital importance in terms of efficiency and of reducing emissions of CO, HC and NO_x in coal gasification power plants. An increase of 50 °C causes a fuel saving during 100 000 operational hours of the same order of magnitude as the investment costs of the gas turbine [1] and, according to [2], a gas turbine inlet temperature above 1250 °C is needed in order to have an economically viable process.

The composition of the corrosive gas for this investigation is chosen to simulate real coal gasification environments as closely as possible, while still maintaining experimental simplicity. The decisive parameters for the simulation gas are the partial pressures of sulphur and oxygen, which should be the same as under service conditions [3]. The equilibrium partial pressures of these species in the gas for the experiments, as well as those in the real environment, are calculated using an in-house computer program, CORGA, based on the minimization of the free energy of the gas system [4].

In the current investigation, attention is focused on the assessment of the effect of corrosion exposure on three aspects of mechanical behaviour: strength, toughness and subcritical crack extension.

2. Experimental procedure

A hot pressed silicon nitride, supplied by CERADYNE Inc., USA, in the form of plates, is used in this study. The material is densified with the aid of Y_2O_3 and Al_2O_3. The determination of density yields an average value of 3.26 $Mg\,m^{-3}$, which proves to be uniform between different plates and different locations within the same plate. The total porosity level is less than 0.1%, and defects larger than 20 μm have not been observed by ultrasonic B-scan and X-ray radiography. X-ray diffraction analysis reveals the presence of β-Si_3N_4 and a minor amount of $Si_3N_4 \cdot 10Y_2O_3 \cdot 9SiO_2$, yttrium silicon oxide nitride (ASTM 30-1462). Transmission electron microscopy (TEM), shows not only the presence of two crystalline phases, but also the presence of a substantial amount of intergranular phase in the amorphous state situated primarily in the triple points between silicon nitride grains (Fig. 1).

Bend specimens with dimensions in millimeters (45 ± 0.5) × (4.0 ± 0.05) × (3.0 ± 0.05), are cut perpendicularly to the hot pressing direction, with all long faces ground parallel to the longitudinal axis. Final finishing is performed with a D46 diamond grinding wheel at a stock removal rate not exceeding 0.025 mm per pass for the last 0.1 mm. This preparation results in a roughness parameter, R_a, of 0.43 ± 0.03 μm measured in the transverse direction and 0.30 ± 0.06 μm in the longitudinal direction. The chevron notch (Fig. 2) is cut by a diamond coated cutting wheel with 100 μm blade thickness and a diameter of 100 mm. A table speed of 10 mm min^{-1} and 5000 r.p.m. allows the slot to be machined in only two steps. The final slot has a width of approximately 160 μm.

0022–2461

Figure 1 TEM micrograph of the as-received material showing the amorphous and crystalline intergranular phase surrounding the hexagonal silicon nitride grains (× 100 000).

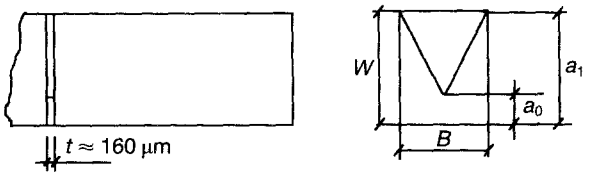

Figure 2 Chevron notch specimen: $W = 4.0 \pm 0.05$ mm, $B = 3.0 \pm 0.05$ mm, $a_0 = 1.4 \pm 0.05$ mm, $a_1 = 4.0 \pm 0.05$ mm.

Corrosion exposure in 0.4% H_2S + 0.75% H_2O + H_2 (balance) atmosphere is performed in an autoclave at 150 Pa for 200 h at 1200 and 1300 °C. In the corrosion jig the specimens are supported by a high purity alumina disc, with drilled holes to minimize the contact surface between the specimens and the support disc. After sealing, the autoclave is filled with flowing active gas and heated at a rate of 10 °C min^{-1}. After reaching the exposure temperature the specimens are held under a gas flow of 17.5 l h^{-1}, for the above mentioned period of time. The water vapour content of the gas is measured at the outlet of the autoclave with a dewpoint meter. To prevent leakage of the gas to the laboratory environment, the active part of the autoclave is surrounded by a protective argon blanket.

The flexure tests are performed in the four point bending mode with outer and inner spans of 40 and 20 mm, respectively. For room temperature tests, a stainless steel jig is used; while the tests at 1200 and 1300 °C are performed on a silicon carbide jig. In both cases, the rollers can rotate freely in their supports. In order not to mask the influence of the corrosive exposure, the high temperature mechanical tests on the corroded and as-received specimens are carried out in an inert nitrogen atmosphere [5]. High temperature tests on exposed material are performed at the same temperature of the exposure conditions. The load is measured by means of a 2 kN load cell with an accuracy of 0.5% and recorded versus crosshead displacement.

3. Results and discussion

After 200 h exposure at high temperature, samples present a weight increase less than 0.2 and 0.7 mg cm^{-2} at 1200 and 1300 °C, respectively, and do not seem to change with further exposure. A light grey scale at 1200 °C, as well as a white one at 1300 °C, appears at the surface with a thickness less than 20 and 100 μm, respectively. A roughness parameter, R_a, of 0.90 ± 0.05 μm is measured in both the transverse and the longitudinal direction. The X-ray diffraction to identify the crystalline phases, presents for the bulk the same results as for the as-received material, whereas for the surface SiO_2 (ASTM 11-695) and $Y_2Si_2O_7$ (ASTM 22-1103) are observed.

From the TEM results it can be concluded that exposure to the sulphidizing environment partially crystallizes the intergranular amorphous phase which is present in the as-received condition, particularly at 1300 °C. However, during the exposure, crystallization occurs primarily in the large pockets at triple points, while along some grain boundaries an amorphous phase can still be identified (Fig. 3).

Figs 4 and 5 are Weibull diagrams showing the strength results from the flexure tests. Twenty specimens have been tested at each condition at a constant displacement rate of 0.5 mm min^{-1}. The parameters of the Weibull distribution (i.e. characteristic strength, σ_0 and modulus, m) have been determined by conventional linear regression analysis using $P_i = (i - 0.5)/n$ as an estimator for the probability of failure, P_f, where i and n, respectively, represent the rank and the total number of specimens.

The high temperature strength values observed in Fig. 4 are smaller than those mentioned in the manufacturer's data sheet, where characteristic strength values in air of 895 MPa at 1200 °C and 500 MPa at 1400 °C are quoted. Oxide strengthening, which is not present in the current experiments, may explain this discrepancy.

Comparing the results obtained on specimens tested as-received and after exposure (Exp.), Fig. 5, it seems that at room temperature the presence of the corroded outer surface layer does not affect the intrinsic failure behaviour of the material [6]. Pre-corrosion at 1300 °C and subsequent mechanical loading at room temperature can thus be considered mutually independent. The simplest approximation consists of neglecting the load bearing capacity of the corrosion layer. Using this approximation and the experimentally observed 16% decrease of the characteristic strength between the exposed and the as-received material (Fig. 5), the average thickness of the corrosion layer in the bend specimens is estimated as 90 μm, which agrees rather well with the average thickness of the corrosion layer observed by light optical microscopy. A similar Weibull modulus is obtained which seems to point towards the existence of the same single population of non-interacting flaws acting as failure initiators in the as-received and exposed specimens. From the fractographs, it appears that the primary mode of crack propagation is transgranular.

As 1300 °C, in spite of the existence of the same oxide layer, approximately the same values of fracture stress are obtained. This in fact represents an effective increase in bend strength by a factor between 1.1 and

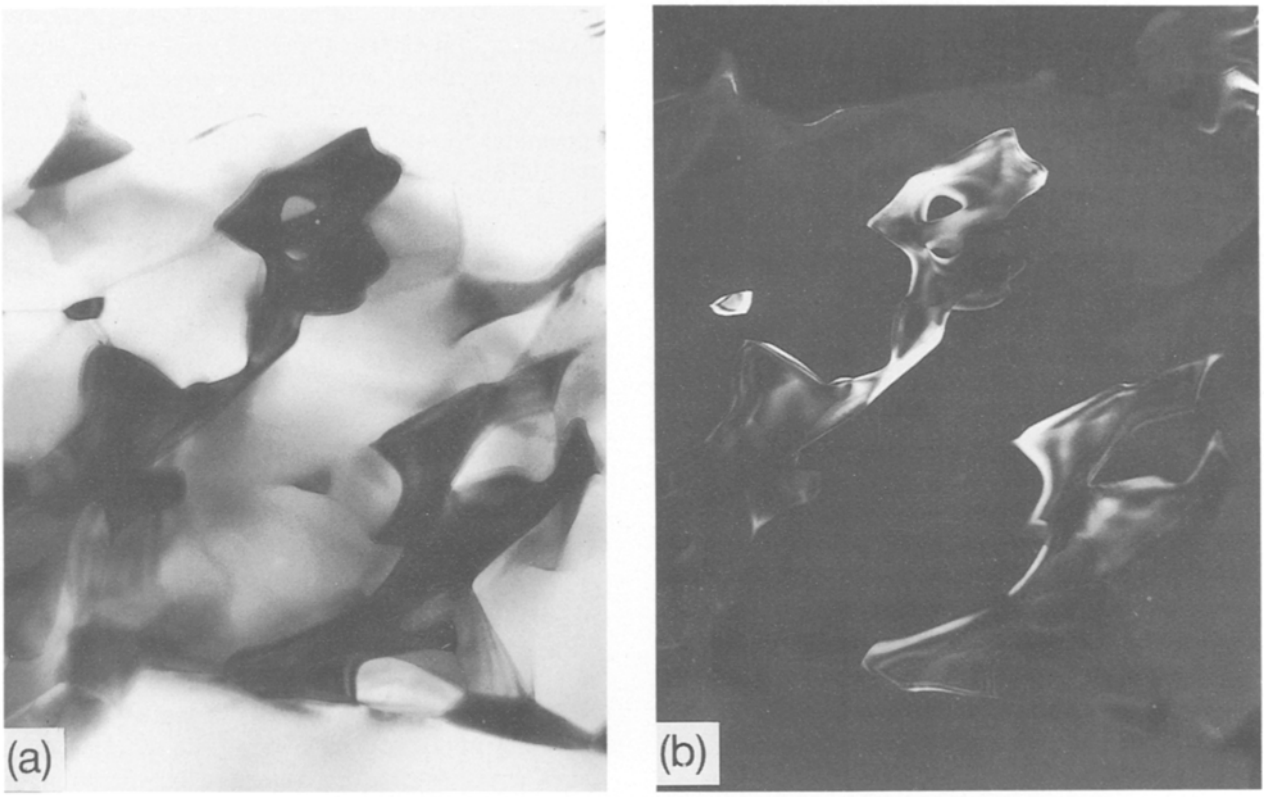

Figure 3 (a) Bright and (b) dark field TEM micrographs of the material after exposure to the sulphidizing environment at 1300 °C showing the increase of crystalline intergranular phase (× 36 000).

T (°C)	m	σ_0 (MPa)	MOR (MPa)
Room temperature	15.8	917	888
1200	17.1	778	755
1300	20.7	608	564

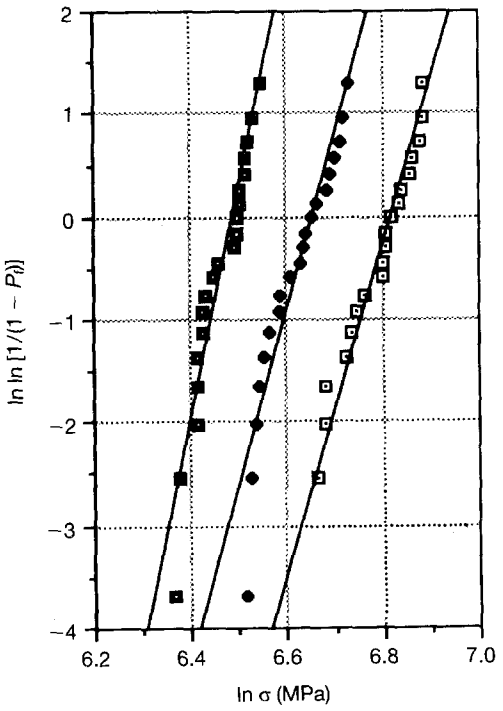

Figure 4 Weibull plot of bend test results on as-received material tested in nitrogen: (⊡) at room temperature, (◆) 1200 °C, and (■) 1300 °C.

T (°C)	m	σ_0 (MPA)	MOR (MPa)
Room temperature, as-received	15.8	917	888
Room temperature, exposed	14.4	771	743
1300, as-received	20.7	608	564
1300, exposed	32.9	613	603

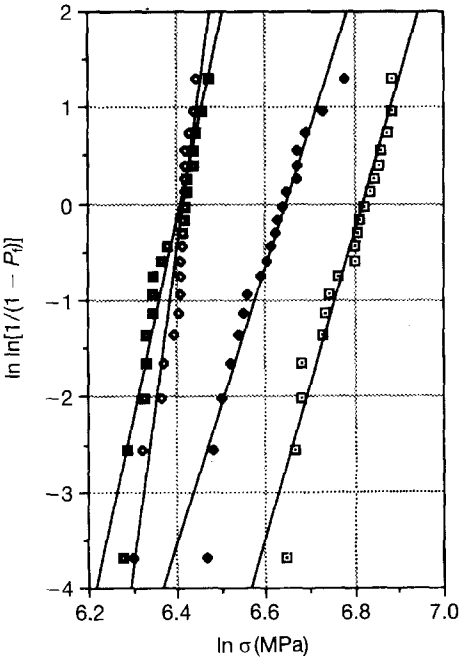

Figure 5 Comparison of bend test results at room temperature and 1300 °C on as-received and exposed specimens: (⊡) room temperature, as-received; (◆) room temperature, exposed; (■) 1300 °C, as-received; and (◆) 1300 °C, exposed.

1.2, which agrees quite well with the results presented by Yamauchi *et al.* [7]. Mechanical strength at high temperature is controlled by the weak intergranular phase, the amount of which is reduced by exposure to the environment. Elongated β-Si_3N_4 hexagonal grains are observed on the fracture surfaces, indicating a predominantly intergranular fracture.

For measuring the temperature dependence of fracture toughness, a chevron notched specimen is used since this technique is considered to be one of the most reliable [8]. The load versus time records of all specimens present a linear behaviour at the beginning of loading, followed by a deviation from this linearity. The deviation occurs before maximum load and is due to crack extension.

Fracture toughness is calculated from the maximum load, P_{max}, by [9]

$$K_{Ic} = \frac{P_{max}}{BW^{1/2}}(2.848 + 6.88\alpha_0 - 2.78\alpha_0^2 + 27.3\alpha_0^3) \times\left(\frac{S_1 - S_2}{W}\right)\left(\frac{\alpha_1 - \alpha_0}{1 - \alpha_0}\right)\left[1 + 0.007\left(\frac{S_1 S_2}{W^2}\right)^{1/2}\right] \quad (1)$$

where $\alpha = a/W$ and S_1, S_2 are the outer and inner spans, respectively.

From Fig. 6 it can be observed that while K_{Ic} of the exposed material slightly decreases with increasing temperature, the fracture toughness of the as-received material shows a maximum at 1300 °C. Since in both situations tests are conducted in an inert nitrogen environment, crack blunting by rapid oxidation is not likely to be the mechanism responsible for this increase [10]. One is inclined to attribute this behaviour to energy dissipation and stress redistribution at the crack tip due to the softening of the glassy phase in the as-received condition [7].

Evaluation of the crack growth behaviour is essential to lifetime prediction. For this purpose dynamic strength tests on plain unnotched specimens and tests on chevron notched specimens, both in four point bending, were performed in order to compare the behaviour of natural and artificial flaws in both as-received and exposed conditions.

Assuming a power law relationship between the crack velocity, v, and the stress intensity factor, K_I, [11]

$$v = A\,K_I^n \quad (2)$$

where A is a constant, and using the LEFM relationship

$$K_I = \sigma Y a^{1/2} \quad (3)$$

where Y is a geometrical factor and a the crack length, the following equation describing the subcritical crack growth behaviour from natural defects in so-called dynamic fatigue tests is obtained [11]

$$\log \sigma_f = B + [1/(n+1)] \log \dot{\sigma} \quad (4)$$

where σ_f is the fracture stress, n is the fatigue parameter, $\dot{\sigma}$ is the imposed stress rate and B is a constant.

A minimum of three specimens have been tested at each stress rate. For the determination of n, the relationship between stress rate and measured fracture stress is fitted in a log–log representation by the least squares method, using three decades for the exposed material and two decades for the as-received. The reason for not including results obtained at the lowest stress rate for the latter material is the occurrence of considerable creep deformation, as evident from the large deflections accumulated during testing at this stress rate.

From Fig. 7, it is observed that both material conditions present a similar value for the slow crack growth coefficient. This can be explained by the fact that it is mainly the amorphous phase along grain boundaries that controls viscous flow, and thus the subcritical crack growth. Consequently, crystallization which mainly occurs at triple points is not expected to affect the crack growth exponent.

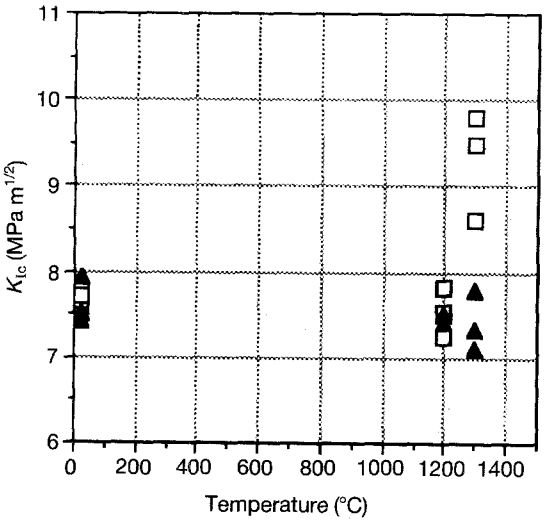

Figure 6 Toughness results obtained on (□) as-received and (▲) exposed specimens.

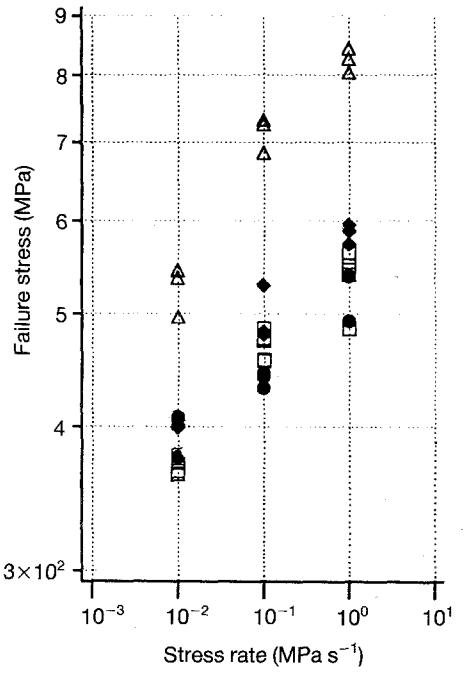

Figure 7 Dynamic bending strength results: (△) 1200 °C as-received, n = 15.1; (□) 1300 °C as-received, n = 13.0; (◆) 1200 °C exposed, n = 13.5; and (●) 1300 °C exposed, n = 13.0.

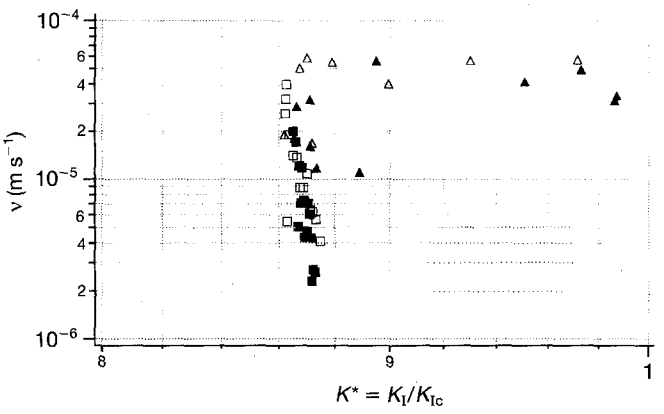

Figure 8 v–K^* diagram of as-received and pre-exposed HP–Si_3N_4: (□) 1200 °C as-received, (△) 1300 °C as-received, (■) 1200 °C exposed, and (▲) 1300 °C exposed.

The subcritical crack growth behaviour can also be determined with a chevron notched specimen according to the following procedure [12, 13].

First of all, the dimensionless compliance, C', of the specimen with a straight-through notch is calculated from

$$\frac{dC'}{d\alpha} = 2\left\{\left(\frac{S_1 - S_2}{W}\right)\left[\frac{3\Gamma\alpha^{1/2}}{2(1-\alpha)^{3/2}}\right]\right\}^2 \quad (5)$$

where

$$\Gamma = 1.9887 - 1.326\alpha - \frac{(3.49 - 0.68\alpha + 1.35\alpha^2)\alpha(1-\alpha)}{(1+\alpha)^2} \quad (6)$$

In a second step, knowing the compliance of unnotched specimens, the relationship between the chevron notch specimen compliance, C_{cn}, and the crack length is calculated from the slice model presented by Bluhm [14], with the help of a FORTRAN computer program [15]

$$\frac{1}{C_{cn}} = \left(\frac{\alpha - \alpha_0}{\alpha_1 - \alpha_0}\right)\left(\frac{1}{C_s\alpha} + \frac{k}{n}\sum_{i=m+1}^{n}\frac{1}{C_s\xi_i}\right) \quad (7)$$

where k is the interlaminar shear factor and $C_s\alpha$ and $C_s\xi$ are the slice compliances.

Finally, the K_I value of the chevron notch specimen is calculated according to

$$K_I = P/BW^{1/2}\left[\frac{1}{2}\left(\frac{dC'_{cn}}{d\alpha}\right)\left(\frac{\alpha_1 - \alpha_0}{\alpha - \alpha_0}\right)\right]^{1/2} \quad (8)$$

where P is the load and $C'_{cn} = E'BC_{cn}$ is the dimensionless compliance with $E' = E$ for plane stress and $E' = E/(1 - \nu^2)$ for plane strain.

Tests at 1200 °C are performed using a crosshead speed of 0.5 mm min^{-1} until 90–95% of the failure load; after that point, the crosshead is kept motionless and the load is recorded versus time. At the above mentioned load level, stable crack growth is easily obtained, resulting in the relaxation curve. At 1300 °C a deviation from linearity is observed at an early stage in the load–displacement curve and this behaviour rules out the use of the previous procedure. In order to overcome this experimental difficulty the change of load corresponding to stable crack growth is measured at a crosshead speed of 0.05 mm min^{-1} up to failure of the specimen.

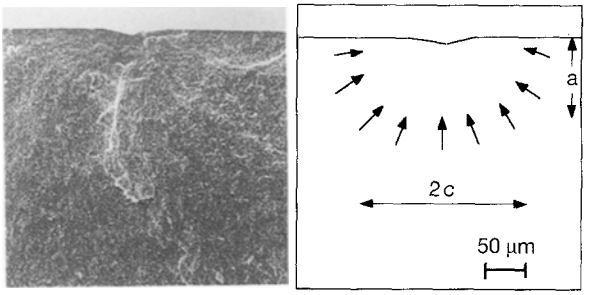

Figure 9 Vicker's indentation crack profile (×200) (ratio crack depth: crack length = 0.8).

The compliance is calculated from the load and the crosshead displacement with a correction for the compliance of the system without specimen.

Over the experimentally covered range at 1300 °C, the v–K* diagram is found to be flat for crack speeds between 3 and 6×10^{-5} m s^{-1}. Data points at lower velocities show that the crack velocity, both at 1200 and 1300 °C, does not increase even when the stress intensity factor increases. This behaviour can be attributed either to an increase in resistance to fracture characterized through the concept of an R-curve or to experimental errors.

In order to clear this question, and also to be able to make long lifetime predictions, the crack velocity range should be extended to lower values. Since the compliance method is restricted to crack propagation rates, $v > 10^{-6}$ m s^{-1}, the indentation induced flaw method is used for this purpose.

Two distinct load dependent crack profiles are known to develop in ceramics by Vicker's indentation: semi-elliptical and Palmquist cracks [16]. For the indentations in this study, crack contour observations reveal a semi-elliptical shape with a ratio of crack depth to crack length of 0.8 (Fig. 9). K_{Ic} values calculated using this shape and the above mentioned ratio are plotted in Fig. 10, as a function of indentation load P_{ind}. Toughness values are load independent for the indentation loads used, and present similar values to those obtained by the chevron notch technique.

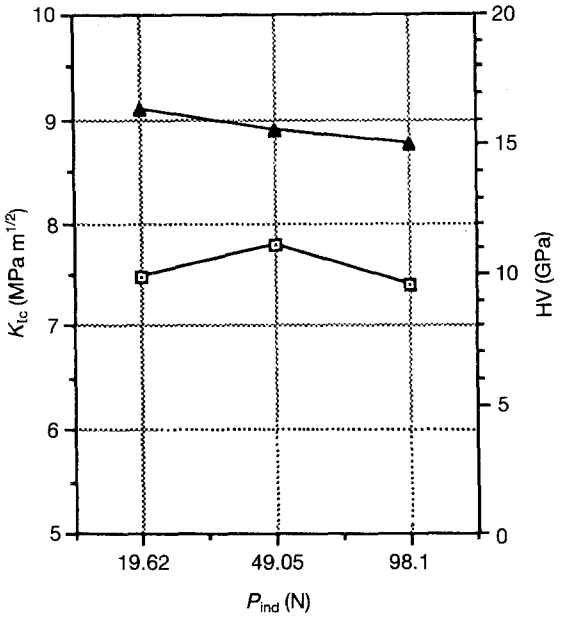

Figure 10 Fracture toughness and Vicker's hardness as a function of the indentation load: (— ⊡ —) K_{Ic} (MPa m$^{1/2}$); (—▲—) HV (GPa).

For crack growth tests the specimen surface is polished with 1 μm diamond paste and a Vicker's indentation is introduced at the centre of the polished surface with a 98 N load and 30 s holding time. The induced flaws are extended by subjecting both as-received and exposed four point bend bars to constant load and temperature in nitrogen for time periods ranging from 30 to 300 min at 1200 and 1300 °C, according to [15]. Loading and unloading is done as quickly as possible in less than 5 s. After a loading time interval, δt, the extension of the Vicker's crack, δa, is measured by scanning electron microscopy (SEM) and the mean crack velocity, v, is calculated according to

$$v = \frac{\delta a}{\delta t} \tag{9}$$

K_I values at the crack tip before and after loading are calculated by

$$K_I = Y\sigma(\pi a/Q)^{1/2} \tag{10}$$

where σ is the applied stress, a the flaw depth, Y the shape factor and $Q^{1/2}$ is an elliptic integral whose value depends on a/c [17, 18].

The average of both K_I values (before and after loading) is used as abscissa in the v–K^* diagram.

The above described method, while very good at room and moderate temperatures [17, 18], becomes inadequate for the present material at 1200 and 1300 °C. Despite the inert nitrogen environment, exposure to high temperature for a period of about 2 h, even without applying any load, renders it impossible to measure accurately the crack length after indentation on the polished surface.

4. Summary

The XRD investigations fail to distinguish the evolution of the crystallization of the amorphous intergranular phase and transmission electron microscopy (TEM) investigations are indispensable. The latter show that the majority of the amorphous phase is located in the triple points between silicon nitride grains and that crystallization starts in these regions. However, along some grain boundaries an amorphous phase can still be identified.

During exposure, and in spite of the low oxygen partial pressure, SiO_2 is quasi-stable and formation of SiS is inhibited by protective SiO_2 [19]. The bulk, however, is subjected to heat treatment at high temperature. This enhances the crystallization and is responsible for the observed increase in strength at high temperature when the crack propagation is predominantly intergranular.

Bend strength tests show that at room temperature a slight reduction in characteristic strength occurs due to a decrease in the dimensions of the load bearing cross-section, equal to the thickness of the corroded outer surface layer. At 1300 °C, however, in spite of the existence of the same oxide layer, approximately the same values of fracture stresses are obtained, before and after corrosion, indicating an increase of the material's strength.

Fracture toughness measurements present similar results at temperatures up to 1200 °C inclusive, and a substantially higher K_{Ic} value of the as-received material at 1300 °C. Since at this temperature both the as-received and exposed material are tested in the same inert environment this different behaviour is tentatively attributed to energy dissipation and stress redistribution at the crack tip due to the softening of the glassy phase.

Differences in crack growth behaviour between both conditions are not observed because an amorphous film along grain boundaries remains. Since it is the thickness of the amorphous film that controls viscous flow, sulphidization does not affect the slow crack growth coefficient. On the other hand the material loses ability to accommodate stresses arising from the viscous flow of the glassy phase between the silicon nitride grains, and this consequently explains the decrease in toughness at high temperature in the exposed condition.

5. Conclusions

Crystallization of the large pockets at triple points makes the cavity formation and growth very difficult. Consequently, longer rupture life times in the pre-exposed condition are to be expected in creep experiments that are presently being carried out under uniaxial tension at 1200 and 1300 °C.

Another area for future research would be, as it is pointed out by [20], the effect of grain size and morphology, because they may affect the importance of the devitrification. Since the microstructure of the exposed material is strongly dependent upon both temperature and time of heat treatment [21], it should be worth clarifying the importance of these parameters.

Finally, the indentation induced flaw method to study the crack growth behaviour of HP–Si_3N_4 at

temperatures of 1200 °C or higher is not recommended. In spite of the inert environment used, the intergranular phase emerges to the surface and hides the real length of the crack, rendering it impossible to study the subcritical crack extension.

Acknowledgements

The authors would like to thank their colleagues G. von Birgelen, V. Harrison and P. Young for their technical assistance. This work has been performed within the research and development programme of the Commission of the European Communities. One of the authors (CSM) wishes to thank the Commission for a grant.

References

1. T. SCHULENBERG, in "Proceedings of the Conference High Temperature Materials for Power Engineering, Liège" (1990), edited by E. Bachelet, R. Brunetaud, D. Coutsouradis, P. Esslinger, J. Ewald, I. Kvernes, Y. Lindblom, D. B. Meadowcroft, V. Regis, R. B. Scarlin, K. Schneider and R. Singer (Kluwer Academic Publishers, Dordrecht, 1990) pp. 903–913.
2. B. J. DAVIDSON, D. B. MEADOWCROFT and J. STRINGER, in "High Temperature Alloys for Gas Turbines and Other Applications", edited by W. Betz, R. Brunetaud, D. Coutsouradis, H. Fischmeister, T. B. Gibbons, I. Kvernes, Y. Lindblom, J. B. Marriott and D. B. Meadowcroft (Reidel Publishing Company, Dordrecht, 1986) pp. 219–244.
3. F. A. COSTA OLIVEIRA, R. A. H. EDWARDS and R. J. FORDHAM, Workshop on High Temperature Corrosion of Advanced Materials (Frankfurt am Main, Germany, 1990).
4. W. B. WHITE, S. N. JOHNSON and G. B. DANTZIG, *J. Chem. Phys.* **28** (1958) 751.
5. C. SARAIVA MARTINS, M. STEEN, L. GUERRA ROSA and J. BRESSERS, in "Proceedings of the International Conference on Fracture Mechanics of Ceramics", Nagoya, Japan, July 1991, edited by R. C. Bradt, A. G. Evans, D. P. H. Hasselman and F. F. Lange (Plenum Press, New York, 1992) Vol. 10, pp. 379–390.
6. *Idem*, in "Proceedings of the Second European Conference on Ceramics, Augsburg, Germany", edited by G. Ziegler and H. Hausner (Deutsch Keramische Gesellschaft e.V., Augsburg, Germany, 1991) Vol. 2, pp. 1357–1361.
7. Y. YAMAUCHI, T. OHJI, W. KANEMATSU, S. ITO and K. KUBO, in "Proceedings of the 30th Japanese Congress on Materials Research" (1991).
8. D. MUNZ, *Int. J. Fracture* **16** (1980) R137.
9. V. A. M. A. S., in "The Proposal of '90 VAMAS High Temperature Fracture Toughness Round Robin Test", instigated by Dr. Hideo Awaji, Japan, Fine Ceramics Centre (1990).
10. D. MUNZ, G. HIMSOLT and J. ESCHWEILER, *J. Amer. Ceram. Soc.* **63** (1980) 341.
11. R. W. DAVIDGE, in "Mechanical Behavior of Ceramics", Cambridge Solid State Science Series, edited by R. W. Cahn, M. W. Thompson and I. M. Ward (Cambridge University Press, London, 1979) p. 144.
12. D. MUNZ, R. T. BUBSEY and J. L. SHANNON Jr, *J. Amer. Ceram. Soc.* **63** (1980) 300.
13. S. SAKAGUCHI, N. MURAYAMA and F. WAKAI, in "Proceedings of the 30th Japanese Congress on Materials Research" (1991).
14. J. BLUHM, *Eng. Fract. Mech.* **7** (1975) 593.
15. Y, YAMAUCHI, in the Report "Comparison of Subcritical Crack Growth Behavior of Monolithic and Composite Ceramic Materials", of the visiting scientist period of Y. Yamauchi at the Institute for Advanced Materials, Joint Research Centre, Petten (1990).
16. A. M. EL ASLABI, G. KLEIST, R. U. STEINBRECH and H. NICKEL, in "Proceedings of the Festigkeitsseminar uber Keramische (verbund-) Werkstofle", (Deutsch Keramische Gesellschaft e.V., Wiesbaden und Berlin, 1991) Vol. 6, pp. 133–149.
17. K. TANAKA, *J. Mater. Sci.* **22** (1987) 1501.
18. M. KAWAI, H. ABE and J. NAKAYAMA, in "Fracture Mechanics of Ceramics", Vol. 6, edited by R. C. Bradt, A. G. Evans, D. P. H. Hasselman and F. F. Lange (Plenum Press, New York, 1983) p. 587.
19. F. COSTA OLIVEIRA, PhD Thesis (Technical University of Delft, The Netherlands, 1992).
20. L. A. PIERCE, D. M. MIESKOWSKI and W. A. SANDERS, *J. Mater. Sci.* **21** (1986) 1345.
21. L. K. L. FALK and G. L. DUNLOP, *ibid.* **22** (1987) 4369.

Received 7 January 1993
and accepted 21 March 1994